


Article

Synthesis of Zn²⁺-Pre-Intercalated V₂O₅·nH₂O/rGO Composite with Boosted Electrochemical Properties for Aqueous Zn-Ion Batteries

Yanzhi Fan ¹, Xiaomeng Yu ², Ziyi Feng ², Mingjie Hu ^{3,*} and Yifu Zhang ^{2,*} ¹ Beijing Aerospace Intelligent Construction Co., Ltd., Beijing 102600, China² State Key Laboratory of Fine Chemicals, School of Chemical Engineering, Dalian University of Technology, Dalian 116024, China³ Hubei Key Laboratory of Advanced Aerospace Propulsion Technology, Hubei Military-Civilian Integration and Co-Innovation Center of Aerospace Propulsion and Materials Technology, Wuhan 430040, China

* Correspondence: humingjie1987@whu.edu.cn (M.H.); yfzhang@dltu.edu.cn (Y.Z.)

Abstract: Layered vanadium-based materials are considered to be great potential electrode materials for aqueous Zn-ion batteries (AZIBs). The improvement of the electrochemical properties of vanadium-based materials is a hot research topic but still a challenge. Herein, a composite of Zn-ion pre-intercalated V₂O₅·nH₂O combined with reduced graphene oxide (ZnVOH/rGO) is synthesized by a facile hydrothermal method and it shows improved Zn-ion storage. ZnVOH/rGO delivers a capacity of 325 mAh·g⁻¹ at 0.1 A·g⁻¹, and this value can still reach 210 mAh·g⁻¹ after 100 cycles. Additionally, it exhibits 196 mAh·g⁻¹ and keeps 161 mAh·g⁻¹ after 1200 cycles at 4 A·g⁻¹. The achieved performances are much higher than that of ZnVOH and VOH. All results reveal that Zn²⁺ as “pillars” expands the interlayer distance of VOH and facilitates the fast kinetics, and rGO improves the electron flow. They both stabilize the structure and enhance efficient Zn²⁺ migration. All findings demonstrate ZnVOH/rGO’s potential as a perspective cathode material for AZIBs.

Keywords: composite materials; Zn_xV₂O₅·nH₂O/rGO; electrochemical properties; energy storage and conversion; Zn-ion batteries



Citation: Fan, Y.; Yu, X.; Feng, Z.; Hu, M.; Zhang, Y. Synthesis of Zn²⁺-Pre-Intercalated V₂O₅·nH₂O/rGO Composite with Boosted Electrochemical Properties for Aqueous Zn-Ion Batteries. *Molecules* **2022**, *27*, 5387. <https://doi.org/10.3390/molecules27175387>

Academic Editor: Minghao Yu

Received: 18 July 2022

Accepted: 19 August 2022

Published: 24 August 2022

Publisher’s Note: MDPI stays neutral with regard to jurisdictional claims in published maps and institutional affiliations.



Copyright: © 2022 by the authors. Licensee MDPI, Basel, Switzerland. This article is an open access article distributed under the terms and conditions of the Creative Commons Attribution (CC BY) license (<https://creativecommons.org/licenses/by/4.0/>).

1. Introduction

Nowadays, environmental problems and the energy crisis have become dominating hot topics. Researchers are engaged in exploring various high-efficiency, green energy storage and conversion devices [1–3]. Among various energy storage systems, aqueous Zn-ion batteries (AZIBs) have attracted increasing interest in recent years as an alternative for grid-scale energy storage systems because of their low-cost, eco-friendliness and safety [4–7]. For AZIBs, metal zinc is typically used as the anode due to its high theoretical capacity of 820 mAh·g⁻¹ and abundance. However, a lot of work is still ongoing aimed at finding suitable cathode materials that meet the requirements of high energy density and long-cycle life [8–10].

So far, various cathode materials for AZIBs, such as manganese oxides, vanadium oxides and their related compounds, Prussian blue analogues, cobalt oxides, organic molecules and so on, have been widely studied [11–16]. Among them, vanadium (V)-based compounds are considered as attractive candidates because of their variable valence states, abundant reserves and open-frame structures [17–21]. This material can accommodate lots of Zn-ions. Layered hydration vanadium pentoxide V₂O₅·nH₂O (abbreviation as VOH) possesses tunable structures and multivalences for large Zn²⁺ reserves and ingress/egress [22–25]. Although many progresses of vanadium oxides are achieved as cathode materials for AZIBs, they still suffer from intrinsic poor electroconductivity and hindered dynamics owing to the

strong electrostatic attraction between Zn^{2+} and VO layer [26]. Thus, the structural engineering of vanadium oxides with open architecture is key to eliminating this electrostatic impact [27].

As the cathode material for AZIBs, $\text{Zn}_{0.25}\text{V}_2\text{O}_5 \cdot n\text{H}_2\text{O}$ was first reported by Nazar's group [28]; it exhibited high capacity (ca. 300 mAh g^{-1} @ 50 mA g^{-1}) and showed excellent rate performance. After that, some objects (e.g., various metal ions, different polymers) are introduced to tune the lamellar structure of VOH. After adjusting the interlayer spacing, electrochemical properties of intercalated VOH were significantly boosted [29–34]. For instance, Liu et al. reported that polyaniline-intercalated VOH shows an expanded interlayer space of $\sim 14 \text{ \AA}$ delivering a capacity of $354 \text{ mAh} \cdot \text{g}^{-1}$ at $0.1 \text{ A} \cdot \text{g}^{-1}$ and good cycle stability [35]. Other reports prove the utility of object-intercalated VOH with enhanced electrochemical properties for AZIBs. Although $\text{Zn}_{0.25}\text{V}_2\text{O}_5 \cdot n\text{H}_2\text{O}$ for AZIBs has been reported, Zn^{2+} -intercalated VOH combined with rGO has been rarely reported to the best of our knowledge [36]. As is well known, recombination rGO with metal oxides enhances the conductivity, facilitates electron flow and stabilizes the structure of the composites [37,38].

Herein, a composite with Zn^{2+} -intercalated VOH integrated with rGO (denoted as ZnVOH/rGO) is developed and it exhibits enhanced Zn-ion storage with a capacity of $325 \text{ mAh} \cdot \text{g}^{-1}$ at $0.1 \text{ A} \cdot \text{g}^{-1}$ and $210 \text{ mAh} \cdot \text{g}^{-1}$ after 100 cycles. The capacity is not higher than that reported by Nazar ($0.05 \text{ A} \cdot \text{g}^{-1}$) because of our value obtained at a very high rate $0.1 \text{ A} \cdot \text{g}^{-1}$. The achieved performances of ZnVOH/rGO are much higher than that of ZnVOH and VOH, and even surpass some state-of-the-art cathodes for the application of AZIBs.

2. Results and Discussion

ZnVOH/rGO was prepared by a hydrothermal route combination with freeze-drying treatment. V-based complexes were first formed by reacting between V_2O_5 and H_2O_2 to form a clear solution [35]. In hydrothermal route, VOH nanobelts were formed, meanwhile, Zn-ions were intercalated into a VOH interlayer, expanding the distance of interlayer spacing, like other metal ions [30]. During this process, GO was transformed to rGO and ZnVOH was connected/fixed with rGO by hydroxyl bonding or electrostatic attraction [38]. ZnVOH/rGO was formed by this hydrothermal route and finally obtained by freeze-drying treatment.

Figure 1 shows the XRD patterns of ZnVOH and ZnVOH/rGO. The characteristic peaks correspond to the standard pattern of $\text{V}_2\text{O}_5 \cdot 1.6\text{H}_2\text{O}$ (JCPDS, card No. 40-1296) [39]. The main peaks of the four materials matched well with PDF#40-1296, but due to the intercalation of metal ions, the peak position of VOH will be shifted. These phenomena are reported in the previous literature [39]. The (001) peak with the lattice spacing of 13.1 \AA is achieved from ZnVOH/rGO, which is larger than the value (11.9 \AA) of ZnVOH. The increase of interlayer spacing not only expands the transport channel of zinc ions, but also weakens the electrostatic interaction with the main material. In order to determine the composition of the materials, we conducted the ICP test for the two materials. The result is shown in Tables S1 and S2. The Zn/V ratios in ZnVOH and ZnVOH/rGO are similar, both about 0.11:1. This is very consistent with the synthesis of ZnVOH/rGO compared with ZnVOH only the addition of rGO. From the test results, it is found that the ratio of Zn to V does not change greatly with the addition of rGO, but the addition of rGO greatly improves the layer spacing. This may be because the introduction of rGO makes more water molecules enter the layer between vanadium oxides. This result suggests the addition of GO can not only facilitate the fast Zn ion transfers but also improve the electrochemical conductivity of ZnVOH [40]. In our experiment, we also investigated the amount of rGO. However, the interlayer spacing of ZnVOH/rGO has changed little with the change of rGO.

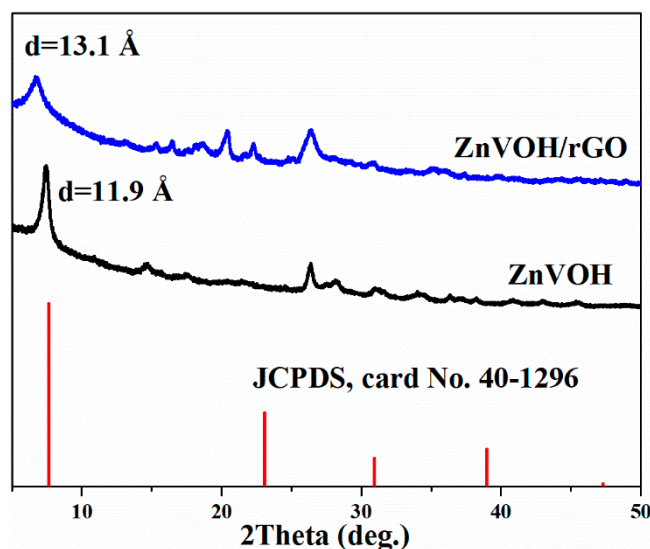


Figure 1. XRD patterns of ZnVOH and ZnVOH/rGO.

Figure 2a depicts FTIR spectra of ZnVOH and ZnVOH/rGO. The characteristic bands at 524, 728 and 836 cm^{-1} are assigned to the stretching vibrations of O-V-O. The bands at 995 and 1015 cm^{-1} are assigned to $\text{V}^{4+} = \text{O}$ and $\text{V}^{5+} = \text{O}$, respectively [41]. Meanwhile, some emerged characteristic bands at 1095, 1147 and 1730 cm^{-1} are observed, which are attributed to the C-H, C-O and C = O bonds from rGO [42]. More structural details of ZnVOH and ZnVOH/rGO are provided by Raman spectra, as depicted in Figure 2b. The Raman peaks below 1000 cm^{-1} are assigned to $(\text{V}_2\text{O}_2)_n$, $\text{V}_3\text{-O}$, V-O-V and V = O from ZnVOH [43]. Figure 2b gives Raman spectra of ZnVOH and ZnVOH/rGO. In ZnVOH/rGO, two characteristic peaks at approximately 1340 and 1580 cm^{-1} observed, which are indexed to D-band and G-band, respectively. These two bands are related to defective carbon atoms (D-band) and ordered carbon atoms (G-band) [38]. The ratio of peak strength of I_D/I_G suggests the carbon defect density [38]. Materials with a larger ratio of I_D/I_G suggest a higher carbon defect density, and a better electrochemical performance [40]. The I_D/I_G value of ZnVOH/rGO is 1.02, which means that the composite has a relative higher carbon defect density. This is conducive to energy storage. Moreover, compared to the ZnVOH, the Raman spectrum of ZnVOH/rGO shows peaks at approximately 2700 cm^{-1} , which is attributed to the second-order peak of the D peak (2D-band). This further demonstrates the existence of graphene layers [44]. The above results suggest the successful preparation of the ZnVOH/rGO composite.

The morphologies of the samples were investigated by SEM and TEM. Figures 3 and S1 show the morphologies of ZnVOH and ZnVOH/rGO, respectively. Both samples show uniform nanowires. As shown in Figure 3a,b, ZnVOH nanowires tightly stick to rGO sheets through chemical bonds or electrostatic attraction (ZnVOH nanowires were shown in Figure S1). The results suggest that ZnVOH nanowires and rGO sheets are dispersed well, endowing the electrical conductivity of ZnVOH nanowires. Furthermore, the element of ZnVOH/rGO is advocated by elemental mapping images, as shown in Figures 3c and S2. The elements V, O, Zn and C are uniformly dispersed in ZnVOH/rGO, in line with the results of XRD, FTIR and Raman. We tested the quality of the ZnVOH/rGO before and after calcination, and the content of rGO was about 7.1%. Figure 3d–f represents the TEM images of ZnVOH/rGO, which also reveal that ZnVOH nanowires are densely anchored on rGO sheets, where the strong interaction with each other is formed. This architecture can effectively restrain the aggregation of rGO through π stacking interactions [45]. An HRTEM image inserted in Figure 3f reveals that the lattice distance of (001) plane is expanded to 13.1 Å, which is in line with XRD observation (Figure 1). All the above results confirm that ZnVOH/rGO with an expanded layer spacing is successfully synthesized. This feature not

only facilitates fast kinetics and efficient ion-transfer, but also enhances structural stability and electrical conductivity [46].

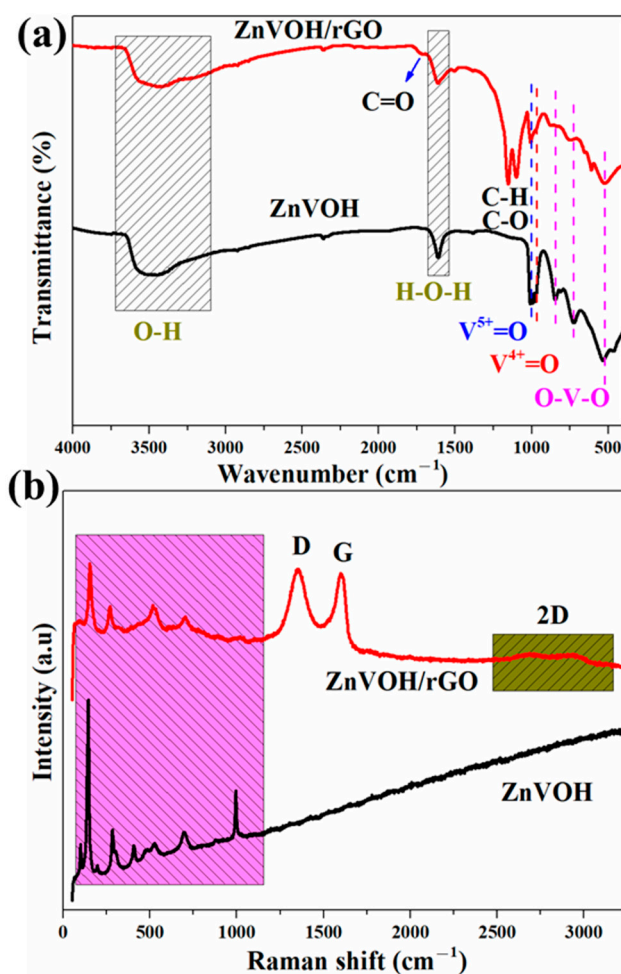


Figure 2. FTIR (a) and Raman (b) spectra of ZnVOH and ZnVOH/rGO.

The Zn-ion storage performance of ZnVOH/rGO was tested (details in Supplementary Material). Figure 4a depicts CV curves of ZnVOH and ZnVOH/rGO at scan rate of $0.1 \text{ mV}\cdot\text{s}^{-1}$ in $0.2\sim 1.4 \text{ V}$ potential range. They have two pairs of redox peaks, and they are assigned to the reactions of $\text{V}^{5+}/\text{V}^{4+}$ and $\text{V}^{4+}/\text{V}^{3+}$, respectively. As for ZnVOH, these two pairs of redox peaks are located at $0.428/0.771 \text{ V}$ and $0.760/1.201 \text{ V}$. However, they are shifted to $0.565/0.752 \text{ V}$ and $0.843/1.045 \text{ V}$ for ZnVOH/rGO. The potential gap of ZnVOH/rGO is much smaller than that of ZnVOH, revealing better redox reaction kinetics and faster ion diffusion leading to the smaller polarization. The above result suggests that the introduction of rGO is good for the redox reaction kinetics, and it also plays a role in promoting thermodynamics [47]. Figure 4b shows the CV curves of ZnVOH/rGO at the initial cycles. These curves are well overlapped, which indicates the excellently reversible Zn^{2+} (de)intercalation of ZnVOH/rGO. Furthermore, two couples of redox peaks in all CV curves (Figure 4) are indexed to ingress/egress of Zn^{2+} , suggesting a multistep intercalation mechanism [29].

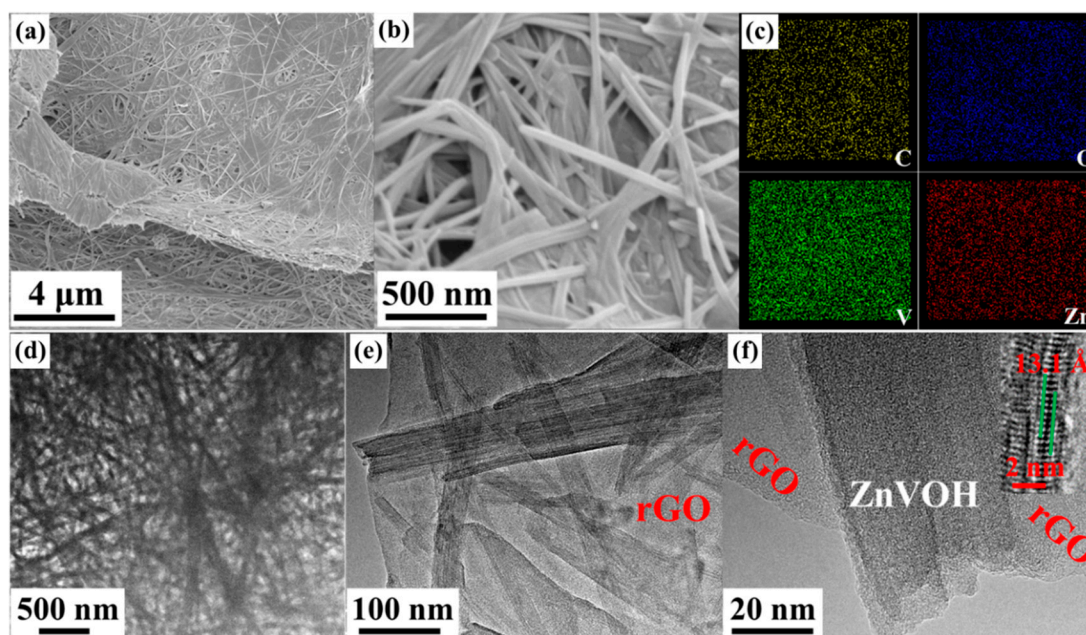


Figure 3. Morphologies of ZnVOH/rGO: (a,b) SEM images; (c) elemental mapping images collected from Figure S2; (d–f) TEM images and a HRTEM image is inserted.

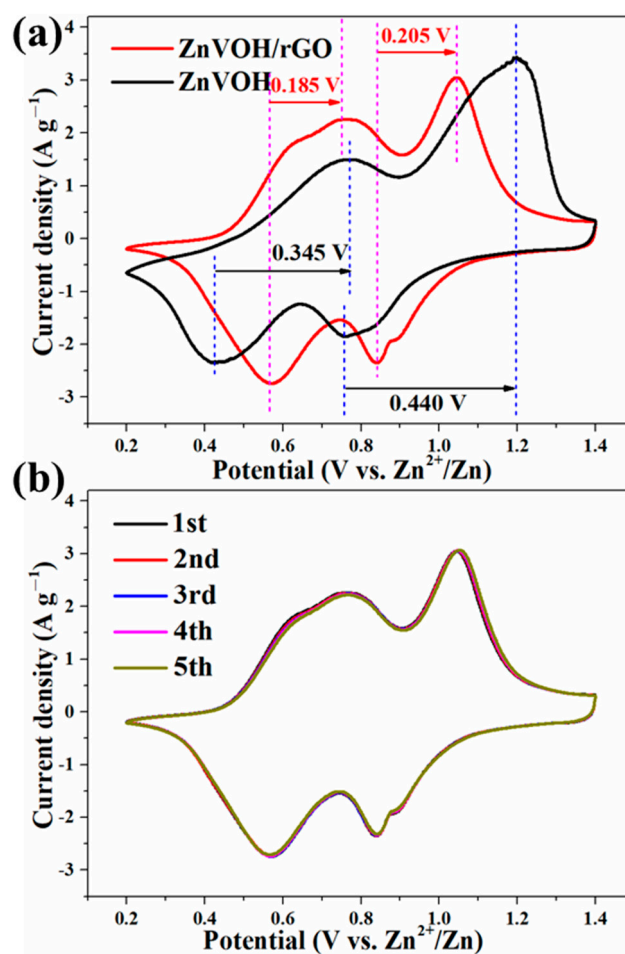


Figure 4. (a) Comparative CV curves of ZnVOH and ZnVOH/rGO; (b) CV curves of ZnVOH/rGO at the first 5 cycles.

Figures 5 and S3 represent GCD curves for different cycles and cycle performances of ZnVOH and ZnVOH/rGO at 0.1 and 4 A·g⁻¹, respectively. There are two voltage plateaus in all GCD curves (Figures 5a and S4a), which well coincide to the multistep intercalation process in CV curves. It is noted that in the ZnVOH/rGO composite we regard ZnVOH and rGO as a whole as the active material to calculate the electrochemical capacity. At 0.1 A·g⁻¹ (Figure 5b), ZnVOH/rGO exhibits a specific capacity of 325 mAh·g⁻¹ and this value still reach 210 mAh·g⁻¹ after 100 cycles, whereas ZnVOH displays lower specific capacity and these two values of ZnVOH are 295 and 140 mAh·g⁻¹. At 4 A·g⁻¹ (Figure S4b), ZnVOH/rGO exhibits a capacity of 196 mAh·g⁻¹ and it retains 161 mAh·g⁻¹ after 1200 cycles, whereas ZnVOH exhibits a capacity of 145 and 126 mAh·g⁻¹. Moreover, the coulombic efficiencies of ZnVOH/rGO are near 100%, which means that ZnVOH/rGO is more stable than ZnVOH (Figures 5b and S4b). The electrochemical performance of the ZnVOH mixture electrode with the same amount of C (carbon black + C coming from rGO), and its electrochemical performance is far inferior to that of ZnVOH/rGO. The results show that the connection of rGO to ZnVOH is conducive to the rapid transfer of electrons [38].

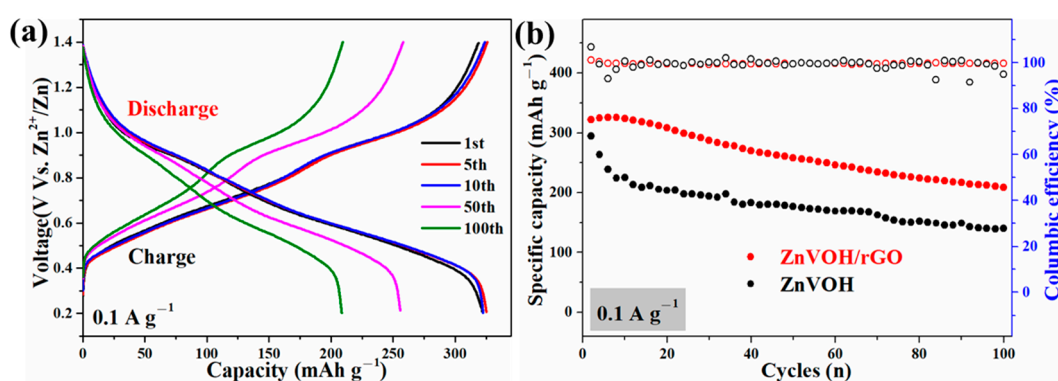


Figure 5. (a) GCD curves of ZnVOH and ZnVOH/rGO; (b) cycle performance of ZnVOH and ZnVOH/rGO at 0.1 A·g⁻¹.

Figure 6 describes the rate performances of ZnVOH and ZnVOH/rGO at 0.1, 0.2, 0.5, 1 and 2 A·g⁻¹ and then returns to 0.1 A·g⁻¹. From the Figure 6, it is clearly seen that ZnVOH/rGO shows higher electrochemical properties compared to ZnVOH. In detail, at 0.1, 0.2, 0.5, 1 and 2 A·g⁻¹, ZnVOH/rGO delivers capacities of 306, 298, 282, 265 and 246 mAh·g⁻¹, respectively. This means, compared with the value at 0.1 A·g⁻¹, the rate retention of ZnVOH/rGO is near 80%. For ZnVOH, this rate retention is approximately 48%. After the current density is back to 0.1 A·g⁻¹, the capacities of ZnVOH/rGO and ZnVOH are 274 and 229 mAh·g⁻¹, respectively, suggesting that these values return to 90% and 86% of the initial values. According to the mass of ZnVOH/rGO, the energy densities of Zn//ZnVOH/rGO cell are calculated to be 249 and 225 Wh·kg⁻¹ at 0.1 and 2 A·g⁻¹, respectively. The above findings reveal that ZnVOH/rGO exhibits much better electrochemical properties (specific capacity, rate and performances) than ZnVOH and VOH [38]. This shows that rGO enhances the rapid electron transport and boosts the electrical conductivity. Furthermore, the achieved performance of ZnVOH/rGO is superior to some recently reported cathodes for AZIBs, as listed in Table S1.

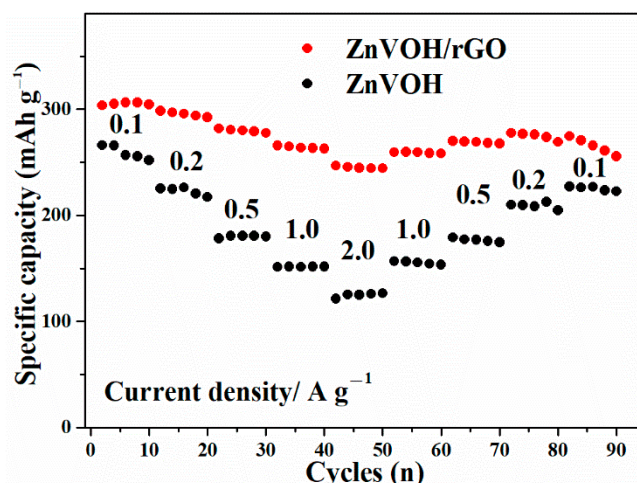


Figure 6. The rate performances of ZnVOH and ZnVOH/rGO.

To better understand why the Zn//ZnVOH/rGO battery has good electrochemical properties, the electrochemical kinetics of Zn//ZnVOH/rGO cell was further studied by CV curves at the scan range of 0.2 to 1.0 $\text{mV}\cdot\text{s}^{-1}$, as shown in Figure 7. The shapes of these shapes of curves are similar and the redox peaks display some shifts and become broader with the scan rate increasing (Figure 7a). The reason for such variation is owing to the polarization effect and can be used to study the detailed kinetic [48]. In general, the empirical power-law relationship between the peak current (i) and scanning rates (v) can be depicted in Equation (1):

$$i = av^b \quad (1)$$

$$\log(i) = \log(a) + b\log(v) \quad (2)$$

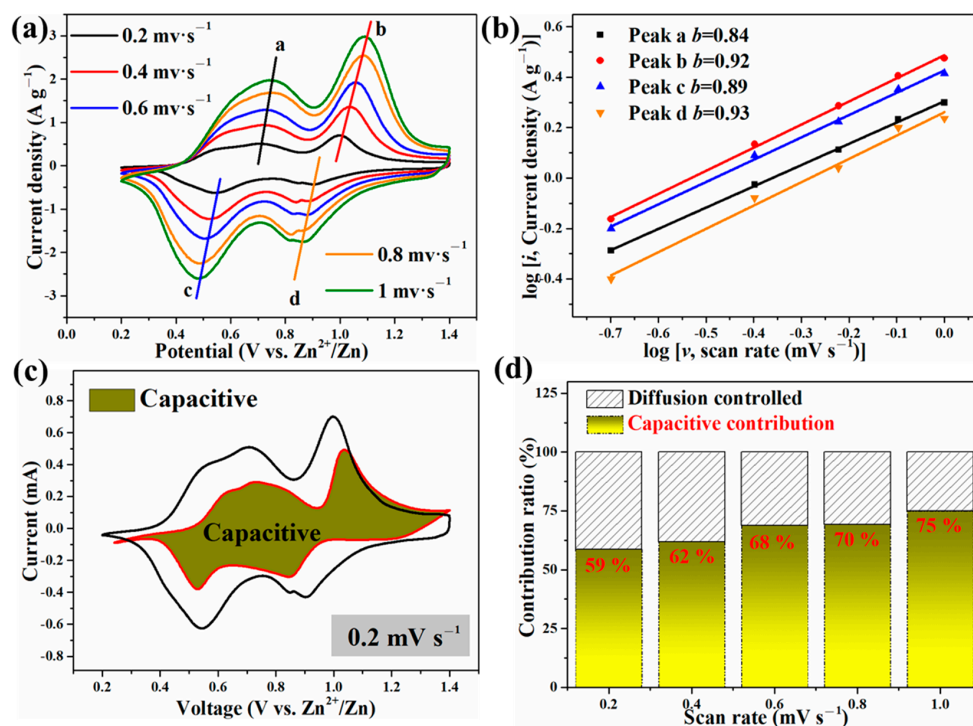


Figure 7. The electrochemical kinetics of Zn//ZnVOH/rGO battery: (a) CV curves at 0.2–1 $\text{mV}\cdot\text{s}^{-1}$, (b) The relationship between \log (sweep rate) and \log (peak current); (c) A typical CV curve with capacitive contribution; (d) capacitive contributions at current densities.

In these two equations [49,50], a and b are parameters. b often ranges from 0.5 (diffusion behavior) to 1 (capacitive behavior) and is related to the charge storage mechanism. To obtain b values, the linear relation between $\log(i)$ and $\log(v)$ is calculated by Equation (2), as represented in Figure 7b. The b values of these four peaks are fitted to be 0.84, 0.92, 0.89 and 0.93, respectively. These b values are near 1, revealing that the capacitive process dominates [22].

The current ($i = av^b$) can be further separated into two parts. The ratio of capacitive behavior is acquired by Equations (3) and (4):

$$i = k_1v + k_2v^{1/2} \quad (3)$$

$$i/v^{1/2} = k_1v^{1/2} + k_2 \quad (4)$$

In these two equations, k_1v represents the capacitive behavior, and $k_2v^{1/2}$ means the diffusion-controlled behavior. The contribution of capacitive behavior is quantitatively reflected by current response at typical voltages, and the representative result at 0.2 mV s^{-1} is shown in Figure 7c. The contribution rates of capacitive behavior are measured to be 59%, 62%, 68%, 70% and 75% at 0.2, 0.4, 0.6, 0.8 and $1 \text{ mV} \cdot \text{s}^{-1}$, respectively. This also reveals the major role of capacitive behavior (Figure 7d).

3. Materials and Methods

All materials are presented in the Supplementary Materials and were used as received. The GO solution was synthesized by the reported improved Hummer's method [24]. To synthesize ZnVOH/rGO, 1 mmol V_2O_5 was dispersed into 36 mL H_2O under vigorous magnetic stirring at room temperature. Then, 1 mL of H_2O_2 (30 wt.%) was slowly dropped into the above solution to obtain a clear orange-red solution. After that, 20 mmol ZnSO_4 and 3.6 mL GO solution (10%) were added, in order. The obtained suspension was further vigorously stirred for 0.5 h. Last, the mixed suspension was sealed in a 50 mL Teflon-lined stainless-steel autoclave and maintained at $120 \text{ }^\circ\text{C}$ for 6 h. After reaction, it was cooled to the room temperature naturally, and dark-green precipitates were obtained by suction filtration and washed with H_2O and freeze-dried for 48 h. For comparison, ZnVOH was prepared without GO solution.

The composition and structure of ZnVOH/rGO were characterized by X-ray diffraction (XRD), Fourier transform infrared spectroscopy (FTIR), Raman spectroscopy, Energy-dispersive X-ray spectrometer (EDS) elemental mapping and inductive coupled plasma emission spectrometer (ICP). Morphology of ZnVOH/rGO was characterized by scanning/transmission electron microscopy (SEM/TEM). The details are represented in the Supplementary Materials.

The cathode was prepared by mixing 80 wt% ZnVOH/rGO, 10 wt% carbon black and 10 wt% polyvinylidene with the N-methyl-2-pyrrolidone as solvent. The slurry was coated onto the above slurry on a clean circular Ti foil (12 mm diameter). After the cathode was dried at $60 \text{ }^\circ\text{C}$ overnight, the 2032-typed AZIB were assembled with glass fiber as the separator, a circular Zn plate of the same dimensions as the anode and $3 \text{ mol L}^{-1} [\text{Zn}(\text{CF}_3\text{SO}_3)_2]$ as the electrolyte. The mass loading of the ZnVOH/rGO is about 2 mg. The electrochemical properties of Zn//ZnVOH/rGO batteries were characterized by cyclic voltammetry (CV), electrochemical impedance spectroscopy (EIS), galvanostatic/intermittent titration technique (GITT) and galvanostatic charge–discharge (GCD) in a potential range of 0.2~1.4 V (vs. Zn^{2+}/Zn).

4. Conclusions

In summary, ZnVOH/rGO was successfully prepared by a facile hydrothermal route. The recombination with rGO can boost the Zn^{2+} storage of Zn^{2+} -pre-intercalated VOH. ZnVOH/rGO exhibits much higher specific capacity, better cycle stability and rate performance than ZnVOH. The achieved performances of ZnVOH/rGO even exceed that of some state-of-the-art cathodes for AZIBs. This is mainly due to: (a) Zn^{2+} in a “pillar” structure

expanding interlayer distance of VOH enhances efficient Zn^{2+} migration, (b) rGO improves the fast electron flow and (c) both materials stabilize the structure.

Supplementary Materials: The following supporting information can be downloaded at: <https://www.mdpi.com/article/10.3390/molecules27175387/s1>, Materials, materials characterizations and electrochemical characterizations. Figure S1: SEM images of ZnVOH. Figure S2: A SEM image of ZnVOH/rGO for collecting elemental mapping images. Figure S3: (a) Cycle performance and (b) GCD curves at $4 \text{ A} \cdot \text{g}^{-1}$ of ZnVOH and ZnVOH/rGO. Table S1: Atomic ratio of Zn and V in ZnVOH by ICP analysis. Table S2: Atomic ratio of Zn and V in ZnVOH/rGO by ICP analysis. Table S3: Comparison of the specific capacities between the previously reported cathode materials for AZIBs and this work [51–62].

Author Contributions: Conceptualization, M.H. and Y.Z.; methodology, Y.F.; software, Y.F.; validation, Y.F., X.Y., Z.F. and Y.Z.; formal analysis, Y.F., X.Y. and Z.F.; investigation, Y.F. and X.Y.; resources; data curation, Y.F. and X.Y.; writing—original draft preparation, Y.F.; writing—review and editing, M.H. and Y.Z.; visualization, Y.F.; supervision, M.H. and Y.Z.; project administration, Y.Z.; funding acquisition, Y.Z. All authors have read and agreed to the published version of the manuscript.

Funding: This research received no external funding.

Institutional Review Board Statement: Not applicable.

Informed Consent Statement: Not applicable.

Data Availability Statement: No information.

Acknowledgments: This work was supported by the Large Instrument and Equipment Open Foundation of Dalian University of Technology.

Conflicts of Interest: The authors declare no conflict of interest.

Sample Availability: No information.

References

1. Zhang, N.; Chen, X.; Yu, M.; Niu, Z.; Cheng, F.; Chen, J. Materials chemistry for rechargeable zinc-ion batteries. *Chem. Soc. Rev.* **2020**, *49*, 4203–4219. [[CrossRef](#)]
2. Chen, X.; Wang, P.; Feng, Z.; Meng, C.; Zhang, Y. Conductive polymer intercalated vanadium oxide on carbon cloth for fast ammonium-ion storage in supercapacitor applications. *Chem. Eng. J.* **2022**, *445*, 136747. [[CrossRef](#)]
3. Wang, P.; Zhang, Y.; Jiang, H.; Dong, X.; Meng, C. Ammonium vanadium oxide framework with stable NH_4^+ aqueous storage for flexible quasi-solid-state supercapacitor. *Chem. Eng. J.* **2022**, *427*, 131548. [[CrossRef](#)]
4. Yang, D.; Tan, H.; Rui, X.; Yu, Y. Electrode Materials for Rechargeable Zinc-Ion and Zinc-Air Batteries: Current Status and Future Perspectives. *Electrochem. Energy Rev.* **2019**, *2*, 395–427. [[CrossRef](#)]
5. Feng, Z.; Sun, J.; Liu, Y.; Jiang, H.; Cui, M.; Hu, T.; Meng, C.; Zhang, Y. Engineering Interlayer Space of Vanadium Oxide by Pyridinesulfonic Acid-Assisted Intercalation of Polypyrrole Enables Enhanced Aqueous Zinc-Ion Storage. *ACS Appl. Mater. Interfaces* **2021**, *13*, 61154–61165. [[CrossRef](#)] [[PubMed](#)]
6. Liu, Y.; Zhang, Y.; Jiang, H.; Sun, J.; Feng, Z.; Hu, T.; Meng, C.; Pan, Z. Synergistic engineering of oxygen-defect and heterojunction boosts Zn^{2+} (De)intercalation kinetics in vanadium oxide for high-performance zinc-ion batteries. *Chem. Eng. J.* **2022**, *435*, 134949. [[CrossRef](#)]
7. Feng, Z.; Sun, J.; Liu, Y.; Jiang, H.; Hu, T.; Cui, M.; Tian, F.; Meng, C.; Zhang, Y. Polypyrrole-intercalation tuning lamellar structure of $\text{V}_2\text{O}_5 \cdot n\text{H}_2\text{O}$ boosts fast zinc-ion kinetics for aqueous zinc-ion battery. *J. Power Sources* **2022**, *536*, 231489. [[CrossRef](#)]
8. Chao, D.; Zhou, W.; Xie, F.; Ye, C.; Li, H.; Jaroniec, M.; Qiao, S.-Z. Roadmap for advanced aqueous batteries: From design of materials to applications. *Sci. Adv.* **2020**, *6*, eaba4098. [[CrossRef](#)]
9. Tie, Z.; Niu, Z. Design Strategies for High-Performance Aqueous Zn/Organic Batteries. *Angew. Chem. Int. Ed.* **2020**, *59*, 21293–21303. [[CrossRef](#)]
10. Liu, S.; Zhu, H.; Zhang, B.; Li, G.; Zhu, H.; Ren, Y.; Geng, H.; Yang, Y.; Liu, Q.; Li, C.C. Tuning the Kinetics of Zinc-Ion Insertion/Extraction in V_2O_5 by In Situ Polyaniline Intercalation Enables Improved Aqueous Zinc-Ion Storage Performance. *Adv. Mater.* **2020**, *32*, 2001113. [[CrossRef](#)]
11. Chen, S.; Li, K.; Hui, K.S.; Zhang, J. Regulation of Lamellar Structure of Vanadium Oxide via Polyaniline Intercalation for High-Performance Aqueous Zinc-Ion Battery. *Adv. Funct. Mater.* **2020**, *30*, 2003890. [[CrossRef](#)]
12. Wan, F.; Zhou, X.; Lu, Y.; Niu, Z.; Chen, J. Energy Storage Chemistry in Aqueous Zinc Metal Batteries. *ACS Energy Lett.* **2020**, *5*, 3569–3590. [[CrossRef](#)]

13. Xu, S.; Sun, M.; Wang, Q.; Wang, C. Recent progress in organic electrodes for zinc-ion batteries. *J. Semicond.* **2020**, *41*, 091704. [[CrossRef](#)]
14. Shi, Y.; Chen, Y.; Shi, L.; Wang, K.; Wang, B.; Li, L.; Ma, Y.; Li, Y.; Sun, Z.; Ali, W.; et al. An Overview and Future Perspectives of Rechargeable Zinc Batteries. *Small* **2020**, *16*, 2000730. [[CrossRef](#)] [[PubMed](#)]
15. Xue, T.; Fan, H.J. From aqueous Zn-ion battery to Zn-MnO₂ flow battery: A brief story. *J. Energy Chem.* **2021**, *54*, 194–201. [[CrossRef](#)]
16. Jiang, H.; Zhang, Y.; Xu, L.; Gao, Z.; Zheng, J.; Wang, Q.; Meng, C.; Wang, J. Fabrication of (NH₄)₂V₃O₈ nanoparticles encapsulated in amorphous carbon for high capacity electrodes in aqueous zinc ion batteries. *Chem. Eng. J.* **2020**, *382*, 122844. [[CrossRef](#)]
17. Liu, S.; Kang, L.; Kim, J.M.; Chun, Y.T.; Zhang, J.; Jun, S.C. Recent Advances in Vanadium-Based Aqueous Rechargeable Zinc-Ion Batteries. *Adv. Energy Mater.* **2020**, *10*, 2000477. [[CrossRef](#)]
18. Jiang, H.; Zhang, Y.; Liu, Y.; Yang, J.; Xu, L.; Wang, P.; Gao, Z.; Zheng, J.; Meng, C.; Pan, Z. In situ grown 2D hydrated ammonium vanadate nanosheets on carbon cloth as a free-standing cathode for high-performance rechargeable Zn-ion batteries. *J. Mater. Chem. A* **2020**, *8*, 15130–15139. [[CrossRef](#)]
19. Feng, Z.; Zhang, Y.; Zhao, Y.; Sun, J.; Liu, Y.; Jiang, H.; Cui, M.; Hu, T.; Meng, C. Dual intercalation of inorganics–organics for synergistically tuning the layer spacing of V₂O₅·nH₂O to boost Zn²⁺ storage for aqueous zinc-ion batteries. *Nanoscale* **2022**, *14*, 8776–8788. [[CrossRef](#)]
20. Zhang, Y.; Xu, L.; Jiang, H.; Liu, Y.; Meng, C. Polyaniline-expanded the Interlayer Spacing of Hydrated Vanadium Pentoxide by the Interface-intercalation for Aqueous Rechargeable Zn-ion Batteries. *J. Colloid Interface Sci.* **2021**, *603*, 641–650. [[CrossRef](#)]
21. Xu, L.; Zhang, Y.; Zheng, J.; Jiang, H.; Hu, T.; Meng, C. Ammonium ion intercalated hydrated vanadium pentoxide for advanced aqueous rechargeable Zn-ion batteries. *Mater. Today Energy* **2020**, *18*, 100509. [[CrossRef](#)]
22. Yan, M.; He, P.; Chen, Y.; Wang, S.; Wei, Q.; Zhao, K.; Xu, X.; An, Q.; Shuang, Y.; Shao, Y.; et al. Water-Lubricated Intercalation in V₂O₅·nH₂O for High-Capacity and High-Rate Aqueous Rechargeable Zinc Batteries. *Adv. Mater.* **2018**, *30*, 1703725. [[CrossRef](#)] [[PubMed](#)]
23. Chen, D.; Rui, X.; Zhang, Q.; Geng, H.; Gan, L.; Zhang, W.; Li, C.; Huang, S.; Yu, Y. Persistent zinc-ion storage in mass-produced V₂O₅ architectures. *Nano Energy* **2019**, *60*, 171–178. [[CrossRef](#)]
24. Sun, J.; Zhang, Y.; Liu, Y.; Jiang, H.; Dong, X.; Hu, T.; Meng, C. Hydrated vanadium pentoxide/reduced graphene oxide-polyvinyl alcohol (V₂O₅·nH₂O/rGO-PVA) film as a binder-free electrode for solid-state Zn-ion batteries. *J. Colloid Interface Sci.* **2021**, *587*, 845–854. [[CrossRef](#)]
25. Zhang, Y.; Chen, A.; Sun, J. Promise and challenge of vanadium-based cathodes for aqueous zinc-ion batteries. *J. Energy Chem.* **2021**, *54*, 655–667. [[CrossRef](#)]
26. Xu, X.; Xiong, F.; Meng, J.; Wang, X.; Niu, C.; An, Q.; Mai, L. Vanadium-Based Nanomaterials: A Promising Family for Emerging Metal-Ion Batteries. *Adv. Funct. Mater.* **2020**, *30*, 1904398. [[CrossRef](#)]
27. Ming, F.; Liang, H.; Lei, Y.; Kandambeth, S.; Eddaoudi, M.; Alshareef, H.N. Layered Mg_xV₂O₅·nH₂O as Cathode Material for High-Performance Aqueous Zinc Ion Batteries. *ACS Energy Lett.* **2018**, *3*, 2602–2609. [[CrossRef](#)]
28. Kundu, D.; Adams, B.D.; Duffort, V.; Vajargah, S.H.; Nazar, L.F. A high-capacity and long-life aqueous rechargeable zinc battery using a metal oxide intercalation cathode. *Nat. Energy* **2016**, *1*, 16119. [[CrossRef](#)]
29. Xia, C.; Guo, J.; Li, P.; Zhang, X.; Alshareef, H.N. Highly Stable Aqueous Zinc-Ion Storage Using a Layered Calcium Vanadium Oxide Bronze Cathode. *Angew. Chem. Int. Ed.* **2018**, *57*, 3943–3948. [[CrossRef](#)]
30. Yang, Y.; Tang, Y.; Liang, S.; Wu, Z.; Fang, G.; Cao, X.; Wang, C.; Lin, T.; Pan, A.; Zhou, J. Transition metal ion-preintercalated V₂O₅ as high-performance aqueous zinc-ion battery cathode with broad temperature adaptability. *Nano Energy* **2019**, *61*, 617–625. [[CrossRef](#)]
31. Yang, Y.; Tang, Y.; Fang, G.; Shan, L.; Guo, J.; Zhang, W.; Wang, C.; Wang, L.; Zhou, J.; Liang, S. Li⁺ intercalated V₂O₅·nH₂O with enlarged layer spacing and fast ion diffusion as an aqueous zinc-ion battery cathode. *Energy Environ. Sci.* **2018**, *11*, 3157–3162. [[CrossRef](#)]
32. Wu, T.; Zhu, K.; Qin, C.; Huang, K. Unraveling the role of structural water in bilayer V₂O₅ during Zn²⁺-intercalation: Insights from DFT calculations. *J. Mater. Chem. A* **2019**, *7*, 5612–5620. [[CrossRef](#)]
33. Wang, M.; Zhang, J.; Zhang, L.; Li, J.; Wang, W.; Yang, Z.; Zhang, L.; Wang, Y.; Chen, J.; Huang, Y.; et al. Graphene-like Vanadium Oxygen Hydrate (VOH) Nanosheets Intercalated and Exfoliated by Polyaniline (PANI) for Aqueous Zinc-Ion Batteries (ZIBs). *ACS Appl. Mater. Interfaces* **2020**, *12*, 31564–31574. [[CrossRef](#)] [[PubMed](#)]
34. Sun, J.; Zhao, Y.; Liu, Y.; Jiang, H.; Huang, C.; Cui, M.; Hu, T.; Meng, C.; Zhang, Y. “Three-in-One” Strategy that Ensures V₂O₅·nH₂O with Superior Zn²⁺ Storage by Simultaneous Protonated Polyaniline Intercalation and Encapsulation. *Small Struct.* **2022**, *3*, 2100212. [[CrossRef](#)]
35. Liu, Y.; Pan, Z.; Tian, D.; Hu, T.; Jiang, H.; Yang, J.; Sun, J.; Zheng, J.; Meng, C.; Zhang, Y. Employing “one for two” strategy to design polyaniline-intercalated hydrated vanadium oxide with expanded interlayer spacing for high-performance aqueous zinc-ion batteries. *Chem. Eng. J.* **2020**, *399*, 125842. [[CrossRef](#)]
36. Mathew, V.; Sambandam, B.; Kim, S.; Kim, S.; Park, S.; Lee, S.; Alfaruqi, M.H.; Soundharrajan, V.; Islam, S.; Putro, D.Y.; et al. Manganese and Vanadium Oxide Cathodes for Aqueous Rechargeable Zinc-Ion Batteries: A Focused View on Performance, Mechanism, and Developments. *ACS Energy Lett.* **2020**, *5*, 2376–2400. [[CrossRef](#)]
37. Pang, Q.; Sun, C.; Yu, Y.; Zhao, K.; Zhang, Z.; Voyles, P.M.; Chen, G.; Wei, Y.; Wang, X. H₂V₃O₈ Nanowire/Graphene Electrodes for Aqueous Rechargeable Zinc Ion Batteries with High Rate Capability and Large Capacity. *Adv. Energy Mater.* **2018**, *8*, 1800144. [[CrossRef](#)]

38. Hu, T.; Feng, Z.; Zhang, Y.; Liu, Y.; Sun, J.; Zheng, J.; Jiang, H.; Wang, P.; Dong, X.; Meng, C. "Double guarantee mechanism" of Ca^{2+} -intercalation and rGO-integration ensures hydrated vanadium oxide with high performance for aqueous zinc-ion batteries. *Inorg. Chem. Front.* **2021**, *8*, 79–89. [[CrossRef](#)]
39. Liu, C.; Neale, Z.; Zheng, J.; Jia, X.; Huang, J.; Yan, M.; Tian, M.; Wang, M.; Yang, J.; Cao, G. Expanded hydrated vanadate for high-performance aqueous zinc-ion batteries. *Energy Environ. Sci.* **2019**, *12*, 2273–2285. [[CrossRef](#)]
40. Wang, X.; Li, Y.; Wang, S.; Zhou, F.; Das, P.; Sun, C.; Zheng, S.; Wu, Z.-S. 2D Amorphous V_2O_5 /Graphene Heterostructures for High-Safety Aqueous Zn-Ion Batteries with Unprecedented Capacity and Ultrahigh Rate Capability. *Adv. Energy Mater.* **2020**, *10*, 2000081. [[CrossRef](#)]
41. Wei, T.; Li, Q.; Yang, G.; Wang, C. Highly reversible and long-life cycling aqueous zinc-ion battery based on ultrathin $(\text{NH}_4)_2\text{V}_{10}\text{O}_{25}\cdot 8\text{H}_2\text{O}$ nanobelts. *J. Mater. Chem. A* **2018**, *6*, 20402–20410. [[CrossRef](#)]
42. Sun, J.; Liu, Y.; Jiang, H.; Dong, X.; Hu, T.; Meng, C.; Zhang, Y. Mn^{2+} as the "spearhead" preventing the trap of Zn^{2+} in layered Mn^{2+} inserted hydrated vanadium pentoxide enables high rate capacity. *J. Colloid Interface Sci.* **2021**, *602*, 14–22. [[CrossRef](#)] [[PubMed](#)]
43. He, P.; Zhang, G.; Liao, X.; Yan, M.; Xu, X.; An, Q.; Liu, J.; Mai, L. Sodium Ion Stabilized Vanadium Oxide Nanowire Cathode for High-Performance Zinc-Ion Batteries. *Adv. Energy Mater.* **2018**, *8*, 1702463. [[CrossRef](#)]
44. Ferrari, A.C.; Meyer, J.C.; Scardaci, V.; Casiraghi, C.; Lazzeri, M.; Mauri, F.; Piscanec, S.; Jiang, D.; Novoselov, K.S.; Roth, S.; et al. Raman Spectrum of Graphene and Graphene Layers. *Phys. Rev. Lett.* **2006**, *97*, 187401. [[CrossRef](#)] [[PubMed](#)]
45. Khazaeli, A.; Godbille-Cardona, G.; Barz, D.P.J. A Novel Flexible Hybrid Battery–Supercapacitor Based on a Self-Assembled Vanadium-Graphene Hydrogel. *Adv. Funct. Mater.* **2020**, *30*, 1910738. [[CrossRef](#)]
46. Zhang, Y.; Chen, M.; Hu, T.; Meng, C. 3D Interlaced Networks of $\text{VO}(\text{OH})_2$ Nanoflakes Wrapped with Graphene Oxide Nanosheets as Electrodes for Energy Storage Devices. *ACS Appl. Nano Mater.* **2019**, *2*, 2934–2945. [[CrossRef](#)]
47. Zheng, J.; Liu, C.; Tian, M.; Jia, X.; Jahrman, E.P.; Seidler, G.T.; Zhang, S.; Liu, Y.; Zhang, Y.; Meng, C.; et al. Fast and reversible zinc ion intercalation in Al-ion modified hydrated vanadate. *Nano Energy* **2020**, *70*, 104519. [[CrossRef](#)]
48. Islam, S.; Alfaruqi, M.H.; Putro, D.Y.; Soundharrajan, V.; Sambandam, B.; Jo, J.; Park, S.; Lee, S.; Mathew, V.; Kim, J. K^+ intercalated V_2O_5 nanorods with exposed facets as advanced cathodes for high energy and high rate zinc-ion batteries. *J. Mater. Chem. A* **2019**, *7*, 20335–20347. [[CrossRef](#)]
49. Zhang, N.; Jia, M.; Dong, Y.; Wang, Y.; Xu, J.; Liu, Y.; Jiao, L.; Cheng, F. Hydrated Layered Vanadium Oxide as a Highly Reversible Cathode for Rechargeable Aqueous Zinc Batteries. *Adv. Funct. Mater.* **2019**, *29*, 1807331. [[CrossRef](#)]
50. Yong, B.; Ma, D.; Wang, Y.; Mi, H.; He, C.; Zhang, P. Understanding the Design Principles of Advanced Aqueous Zinc-Ion Battery Cathodes: From Transport Kinetics to Structural Engineering, and Future Perspectives. *Adv. Energy Mater.* **2020**, *10*, 2002354. [[CrossRef](#)]
51. Wei, T.; Li, Q.; Yang, G.; Wang, C. An electrochemically induced bilayered structure facilitates long-life zinc storage of vanadium dioxide. *J. Mater. Chem. A* **2018**, *6*, 8006–8012. [[CrossRef](#)]
52. Dai, X.; Wan, F.; Zhang, L.; Cao, H.; Niu, Z. Freestanding graphene/ VO_2 composite films for highly stable aqueous Zn-ion batteries with superior rate performance. *Energy Storage Mater.* **2018**, *17*, 143–150. [[CrossRef](#)]
53. Chen, X.; Wang, L.; Li, H.; Cheng, F.; Chen, J. Porous V_2O_5 nanofibers as cathode materials for rechargeable aqueous zinc-ion batteries. *J. Energy Chem.* **2019**, *38*, 20–25. [[CrossRef](#)]
54. Wang, X.; Xi, B.; Ma, X.; Feng, Z.; Jia, Y.; Feng, J.; Qian, Y.; Xiong, S. Boosting Zinc-Ion Storage Capability by Effectively Suppressing Vanadium Dissolution Based on Robust Layered Barium Vanadate. *Nano Lett.* **2020**, *20*, 2899–2906. [[CrossRef](#)] [[PubMed](#)]
55. Lan, B.; Tang, C.; Chen, L.; Zhang, W.; Tang, W.; Zuo, C.; Fu, X.; Dong, S.; An, Q.; Luo, P. $\text{FeVO}_4\cdot n\text{H}_2\text{O}/\text{rGO}$ nanocomposite as high performance cathode materials for aqueous Zn-ion batteries. *J. Alloys Compd.* **2020**, *818*, 153372. [[CrossRef](#)]
56. Chen, L.; Yang, Z.; Wu, J.; Chen, H.; Meng, J. Energy storage performance and mechanism of the novel copper pyrovanadate $\text{Cu}_3\text{V}_2\text{O}_7(\text{OH})_2\cdot 2\text{H}_2\text{O}$ cathode for aqueous zinc ion batteries. *Electrochimica Acta* **2019**, *330*, 135347. [[CrossRef](#)]
57. Li, S.; Chen, M.; Fang, G.; Shan, L.; Cao, X.; Huang, J.; Liang, S.; Zhou, J. Synthesis of polycrystalline $\text{K}_{0.25}\text{V}_2\text{O}_5$ nanoparticles as cathode for aqueous zinc-ion battery. *J. Alloys Compd.* **2019**, *801*, 82–89. [[CrossRef](#)]
58. Alfaruqi, M.H.; Mathew, V.; Song, J.; Kim, S.; Islam, S.; Pham, D.T.; Jo, J.; Kim, S.; Baboo, J.P.; Xiu, Z.; et al. Electrochemical Zinc Intercalation in Lithium Vanadium Oxide: A High-Capacity Zinc-Ion Battery Cathode. *Chem. Mater.* **2017**, *29*, 1684–1694. [[CrossRef](#)]
59. Cai, Y.; Liu, F.; Luo, Z.; Fang, G.; Zhou, J.; Pan, A.; Liang, S. Pilotaxitic $\text{Na}_{1.1}\text{V}_3\text{O}_{7.9}$ nanoribbons/graphene as high-performance sodium ion battery and aqueous zinc ion battery cathode. *Energy Storage Mater.* **2018**, *13*, 168–174. [[CrossRef](#)]
60. Guo, X.; Fang, G.; Zhang, W.; Zhou, J.; Shan, L.; Wang, L.; Wang, C.; Lin, T.; Tang, Y.; Liang, S. Mechanistic Insights of Zn^{2+} Storage in Sodium Vanadates. *Adv. Energy Mater.* **2018**, *8*, 1801819. [[CrossRef](#)]
61. Xia, C.; Guo, J.; Lei, Y.; Liang, H.; Zhao, C.; Alshareef, H.N. Rechargeable Aqueous Zinc-Ion Battery Based on Porous Framework Zinc Pyrovanadate Intercalation Cathode. *Adv. Mater.* **2020**, *32*, e1907798. [[CrossRef](#)] [[PubMed](#)]
62. Chao, D.; Zhu, C.; Song, M.; Liang, P.; Zhang, X.; Tjep, N.H.; Zhao, H.; Wang, J.; Wang, R.; Zhang, H.; et al. A High-Rate and Stable Quasi-Solid-State Zinc-Ion Battery with Novel 2D Layered Zinc Orthovanadate Array. *Adv. Mater.* **2018**, *30*, e1803181. [[CrossRef](#)] [[PubMed](#)]